WHERE DO GALAXIES END?

J. Michael Shull

CASA, Department of Astrophysical & Planetary Sciences, University of Colorado, Boulder, CO 80309, USA

and Institute of Astronomy, University of Cambridge, Cambridge, CB3 0HA, UK

michael.shull@colorado.edu

ABSTRACT

Our current view of galaxies considers them as systems of stars and gas embedded in extended halos of dark matter, much of it formed by the infall of smaller systems at earlier times. The true extent of a galaxy remains poorly determined, with the "virial radius" ($R_{\rm vir}$) providing a characteristic separation between collapsed structures in dynamical equilibrium and external infalling matter. Other physical estimates of the extent of gravitational influence include the gravitational radius, gas accretion radius, and "galactopause" arising from outflows that stall at 100-200 kpc over a range of outflow parameters and confining gas pressures. Physical criteria are proposed to define bound structures, including a more realistic definition of $R_{\rm vir}(M_*, M_h, z_a)$ for stellar mass M_* and halo mass M_h, half of which formed at "assembly redshifts" ranging from $z_a \approx 0.7 - 1.3$. We estimate the extent of bound gas and dark matter around L^* galaxies to be $\sim$ 200 kpc. The new virial radii, with mean $\langle R_{\rm vir} \rangle \approx 200$ kpc, are 40-50% smaller than values estimated in recent HST/COS detections of H I and O VI absorbers around galaxies. In the new formalism, the Milky Way stellar mass, $\log M_* = 10.7 \pm 0.1$, would correspond to $R_{\rm vir} = 153^{+25}_{-16}$ kpc for half-mass halo assembly at $z_a = 1.06 \pm 0.03$. The frequency per unit redshift of low-redshift O VI absorption lines in QSO spectra suggests absorber sizes $\sim$ 150 kpc when related to intervening $0.1L^*$ galaxies. This formalism is intended to clarify semantic differences arising from observations of extended gas in galactic halos, circumgalactic medium (CGM), and filaments of the intergalactic medium (IGM). Astronomers should refer to *bound gas* in the galactic halo or CGM, and *unbound* gas at the CGM-IGM interface, on its way into the IGM.

Subject headings: galaxies: structure — intergalactic medium — ISM: structure

1. INTRODUCTION

Over the last several decades, with new evidence, the objects we call "galaxies" have become much larger. Extended dark-matter "halos" were proposed to produce flat rotation curves at large radii in disk galaxies (Rubin et al. 1980), and a "corona" of hot interstellar gas at the galaxy's virial temperature was predicted by Spitzer (1956) to provide pressure confinement of high-latitude clouds. More recently, astronomers have observed Galactic kinematic tracers (blue horizontal branch stars, globular clusters, satellite galaxies) to distances of 50-250 kpc, and X-ray absorption-line (O VII) spectroscopy has provided evidence of large reservoirs of hot ionized gas in Milky Way halo (cf., Miller & Bregman 2013) and the outskirts of external galaxies (Anderson et al. 2013). In ultraviolet spectroscopy, the Cosmic Origins Spectrograph (COS) on the *Hubble Space Telescope* (HST) has recently detected extended (100-150 kpc) reservoirs of highly ionized oxygen (O VI) around star-forming galaxies (Tumlinson et al. 2011, 2013; Stocke et al. 2013) likely created by outflows of metal-enriched gas from star formation.

Thus, our picture of galaxies has evolved to a system of stars and gas embedded in an extended dark-matter halo, often associated with an even larger gaseous circumgalactic medium (CGM). Galaxies must also be viewed in a cosmological context, in which most of the baryonic matter in the universe is distributed through the intergalactic medium (IGM) in a "cosmic web" shaped by dark-matter structure and inefficient galaxy formation (Cen & Ostriker 1999; Davé et al. 1999; Smith et al. 2011). Observations and modeling (Shull et al. 2012) suggest that 60-80% of the cosmological baryons reside in the low-redshift, multiphase IGM, with perhaps 20% in collapsed form (galaxies, groups, clusters). Although these baryon fractions have some uncertainty, current research is devoted to understanding the physical conditions, spatial extent, and evolution of the gas at distances of 100 kpc to a few Mpc from galaxies. At low redshift ($z \leq 0.4$) the influence of galactic winds and metal injection out to ~ 1 Mpc has been inferred from the association of QSO absorption systems of H I and O VI with nearby galaxies (Penton et al. 2002; Prochaska et al. 2011; Stocke et al. 2006, 2013). Galactic outflows have been detected in absorption toward intermediate-redshift galaxies (Steidel et al. 2004; Martin et al. 2012; Tripp et al. 2011), while at higher redshifts, $z \approx 2.0 - 2.8$, Rudie et al. (2012) found an enhancement of circumgalactic (≤ 300 kpc) H I absorbers in a sample of 886 star-forming galaxies probed by 15 background QSOs. Thus, the connection between galaxies and extended absorption systems seems secure.

Perhaps because of the recent nature of these discoveries, a semantic problem has arisen regarding the proposed structures: halo, CGM, IGM. When does gas cease to be circumgalactic and become intergalactic? Are the edges of galaxies defined by gravity or gas outflows? Are quasar absorption lines the extended halos of intervening galaxies (Bahcall & Spitzer

1969) or filaments of intergalactic gas (Sargent et al. 1980)? Similarly, the phrase "circumgalactic medium" appears to have replaced the concept of a "gaseous halo" or "galactic corona" of hot interstellar gas at the galaxy's virial temperature. Ionized gas with high covering factor has been detected above the Galactic disk in UV absorption-line surveys in metal ions such as O VI (Sembach et al. 2003) and Si III (Shull et al. 2009; Lehner & Howk 2011) and in soft X-ray absorption lines of O VII or O VIII at $z \sim 0$ (Nicastro et al. 2002; McKernan et al. 2005; Wang et al. 2005). The UV absorbers appear to come primarily from gas within 2-10 kpc of the disk plane, elevated by supernovae and star formation in the disk. The Galactic X-ray absorption suggests hot gas at $T \approx 10^{6.3\pm0.2}$ K, but its radial extent is controversial. It may come from a 50-kpc halo (Anderson & Bregman 2010; Gupta et al. 2012) although O VII absorption toward background AGN (Fang et al. 2006; Hagihara et al. 2010) and X-ray binaries (Yao & Wang 2005; Hagihara et al. 2011) suggests that much of the absorption comes within several kpc of the disk. The disk model is consistent with both X-ray observations and total mass considerations (Collins et al. 2005; Fang et al. 2006).

The intent of this paper is to improve the definition of galaxy halos as regions of strong gravitational influence, using dynamical principles and observational constraints. Section 2 discusses physical measures of the spatial extent of large ($\sim L^*$) galaxies including the Milky Way and Andromeda. We discuss the somewhat arbitrary and occasionally misused definition of "virial radius". Somewhat better defined are the "gravitational radius", $GM^2/|W|$, derived from galactic mass and potential energy, the gravitational sphere of influence, accretion radius, and tidal radius. Section 2.3 develops a physically realistic definition of $R_{\rm vir}(M_h, z_a)$ for halos of mass M_h, assembled primarily at redshifts $z_a \approx 0.7 - 1.3$ with further mass accretion down to the present epoch. These new virial radii are typically 50-60% the sizes used to analyze hot halo gas with HST/COS. Section 3 discusses four estimates of galaxy extent: (1) recent kinematical studies of the Milky Way and Andromeda (M31); (2) the "galactopause" where outflow ram pressure balances thermal pressure of the CGM; (3) QSO absorber cross sections derived from metal absorption-line frequency in redshift; and (4) virial radii and halo masses obtained from galaxy abundance-matching. We also discuss recent estimates of the mass and size of the Milky Way and Andromeda halos from kinematics of stars, galactic satellites, and the Local Group. Most of our estimates suggest a smaller spatial extent (~ 200 kpc) for galaxies of mass $\sim 10^{12}\ M_\odot$, comparable to the Milky Way and M31. Section 4 concludes with applications of the new definition of virial radius to observations of extended gas around galaxies made with HST/COS, and to recent mass and size measurements for the Milky Way and M31.

2. DEFINITIONS OF GALAXY EXTENT

This section begins with an overview of the cosmological context, in which galaxies form from density perturbations that turn around from the Hubble expansion background and collapse into dynamical (virial) equilibrium, but with continued infall of dark matter and gas. The environment of these structures will be influenced by "feedback" from star formation within galaxies, through outflows that escape to the IGM or become stalled and return to the galaxy. Both infall and outflow processes depend on the gravitational attraction of the galaxy and its halo, as measured by parameters such as escape velocity, accretion radius, and tidal radius. Below, these measures of gravitational influence are explored, leading to a practical definition of virial radius, consistent with collapse in the past ($z \approx 1$) with continued mass infall to the present.

In a marginally closed, matter-dominated universe ($\Omega_0 = 1$) the classic overdensity $\Delta_{\rm vir} = 18\pi^2 \approx 178$ (often rounded to 200) was derived analytically for a spherical top-hat density perturbation in an Einstein-deSitter universe. The mean background density, $\bar{\rho}(t) \propto t^{-2}$, following the behavior of the expansion parameter $a(t) \propto t^{2/3}$. The perturbation begins its collapse at a "turn-around" density, $\bar{\rho}_{\rm turn} = (9\pi^2/16)\bar{\rho}_m \approx 5.55\bar{\rho}_m$, at a redshift $z_{\rm turn}$. The Local Group halo mass M_h, can be associated with a proper size at turnaround,

$$R_{\rm turn} \approx \left[\frac{M_h}{(4\pi/3)\,(5.55)\,\bar{\rho}_m(z)}\right]^{1/3} \approx (1.2\ {\rm Mpc}) \left(\frac{M_{\rm LG}}{5\times10^{12}\ M_\odot}\right)^{1/3} \left[\frac{1.5}{1+z_{\rm turn}}\right] . \quad (1)$$

Here, we have scaled to the local group mass, $M_{\rm LG} \approx 5 \times 10^{12}\ M_\odot$ at a turnaround redshift $z_{\rm turn} \approx 0.5$, corresponding to the recently measured dynamical history of the Milky Way and Andromeda system (van der Marel et al. 2012). These galaxies turned around from the Hubble flow even earlier, perhaps at $z \approx 2-3$, and had correspondingly smaller radii, probably $0.25 - 0.30$ Mpc. The fact that a given galaxy halo is assembled over a range of redshifts suggests an improved definition of virial radius, $R_{\rm vir}(M_h, z, z_a)$, for a galaxy observed at redshift z but assembled primarily at redshift $z_a > z$, when half its halo mass had collapsed. This change in definition increases the background matter density, $\rho_m(z_a)$, and makes the virial radii smaller. We return to this new formalism in Sections 2.3 and 3.4.

2.1. Gravitational Radius

For extended self-gravitating systems without a sharp boundary, it is useful to define a characteristic "gravitational radius" (Binney & Tremaine 2008) as $r_g = GM^2/|W|$, where W is the gravitational potential energy,

$$W = \frac{1}{2}\int d^3\mathbf{x}\,\rho(\mathbf{x})\,\Phi(\mathbf{x}) = -4\pi G\int_0^\infty \rho(r)\,M(r)\,r\,dr\ . \tag{2}$$

The gravitational radius also bears a close relation to the "half-light radius", r_h, defined by Spitzer (1969) for spherical stellar systems. For many mass distributions, $r_h/r_g = 0.4 - 0.5$, so that $r_h \approx 0.45(GM^2/|W|)$ and $\langle v^2\rangle \approx GM/r_g$. For example, a homogeneous sphere of mass M and radius R has $W = -3GM^2/5R$ and $r_g = 5R/3$. For the density distribution of Plummer's model, $\rho(r) = (3M/4\pi b^3)[1 + (r/b)^2]^{-5/2}$, $W = -(3\pi GM^2/32b)$ and $r_g \approx 3.40b$, where b is the Plummer scale length.

The structure of collapsed halos has been well studied through cosmological N-body simulations (Navarro, Frenk, & White 1997; Springel et al. 2005; Klypin et al. 2011). These numerical experiments show that dark-matter halos collapse into structures with cuspy cores and extended halos. The collapsed structures in these simulations have been fitted to various radial profiles, such as NFW (Navarro, Frenk, & White 1997), for which the density, potential, and enclosed mass are,

$$\rho(r) = \frac{\rho_0}{(r/r_s)\left[1 + (r/r_s)\right]^2} \tag{3}$$

$$\Phi(r) = -\left(4\pi G\rho_0 r_s^2\right)\frac{\ln(1 + r/r_s)}{r/r_s} \tag{4}$$

$$M(r) = \left(4\pi\rho_0 r_s^3\right)\left[\ln\left(1 + \frac{r}{r_s}\right) - \frac{r/r_s}{1 + r/r_s}\right]\ . \tag{5}$$

Here r_s is a characteristic radius defined by the break in slope and related to the virial radius through $r_s = R_{\rm vir}/c$, with the "concentration parameter", c, typically between 5–20. The mass enclosed with the virial radius is written as

$$M_{\rm vir} \equiv M(R_{\rm vir}) = \left(4\pi\rho_0 r_s^3\right)\left[\ln(1 + c) - \frac{c}{1 + c}\right]\ . \tag{6}$$

Increasing the concentration, c, adds mass and extent to the halo. For example, changing c from 5 to 20 doubles the enclosed mass, $M_{\rm vir}(c = 20)/M_{\rm vir}(c = 5) \approx 2.18$. The circular velocity, $V_c^2(r) = GM(r)/r$, reaches a maximum $V_{\rm max}$ at radius $r = 2.1626r_s = 2.1626R_{\rm vir}/c$, and equal to

$$V_{\rm max}^2 = \left(\frac{GM_{\rm vir}}{R_{\rm vir}}\right)\frac{0.2162\,c}{\left[\ln(1 + c) - \frac{c}{1+c}\right]}\ . \tag{7}$$

For the NFW model, the mass diverges logarithmically with radius, and the gravitational radius is formally undefined without a cut-off. By integrating Equation (2) out to the virial radius, $R_{\rm vir} = cr_s$, we can define a finite NFW potential energy and gravitational radius,

$$W_{\rm vir}^{\rm (NFW)} = -\left(\frac{GM_{\rm vir}^2}{2\,r_s}\right) \frac{\left[1 - \frac{\ln(1+c)}{(1+c)} - \frac{1}{(1+c)}\right]}{\left[\ln(1+c) - \frac{c}{1+c}\right]^2} \tag{8}$$

$$r_g^{\rm (NFW)} = GM_{\rm vir}^2/|W_{\rm vir}| = (2r_s)\,\frac{\left[\ln(1+c) - \frac{c}{1+c}\right]^2}{\left[1 - \frac{\ln(1+c)}{(1+c)} - \frac{1}{(1+c)}\right]}\,. \tag{9}$$

This NFW gravitational radius ranges from $r_g = 3.44r_s = 0.69R_{\rm vir}$ (for $c = 5$) to $r_g = 10.8r_s = 0.54R_{\rm vir}$ (for $c = 20$). Table 1 summarizes the ratio of gravitational radius to characteristic scale lengths for several commonly used density distributions.

2.2. Gravitational Radius of Influence and Accretion Radius

Another characteristic radius is the gravitational "radius of influence" (Ferrarese & Ford 2005; Binney & Tremaine 2008) defined as the radius at which the Kepler velocity around a central mass M equals the transverse velocity dispersion, $\sigma_\parallel$, of surrounding stars,

$$R_{\rm infl} = \frac{GM}{\sigma_\parallel^2} = (191\ {\rm kpc}) M_{12}\,\sigma_{150}^{-2}\,. \tag{10}$$

Here, we have approximated the inner portions of the galaxy as a centrally concentrated mass $M = (10^{12}\ M_\odot)M_{12}$ surrounded by outer halo stars with $\sigma_\parallel = (150\ {\rm km\ s^{-1}})\sigma_{150}$. There will be a dynamical dependence of σ on mass M, typically $\sigma \propto M^{0.25-0.30}$.

This formula is analogous to that used in Bondi accretion of gas with isothermal sound speed c_s, for which one defines an "accretion radius"

$$R_{\rm accr} = \frac{2GM}{c_s^2} = (202\ {\rm kpc}) M_{12}\,T_{6.5}^{-1}\,. \tag{11}$$

Here again, we have scaled to a $10^{12}\ M_\odot$ galaxy surrounded by a gaseous halo at its virial temperature $T = (10^{6.5}\ {\rm K})T_{6.5}$ with $c_s = (kT/\mu)^{1/2} = (207\ {\rm km\ s^{-1}})T_{6.5}^{1/2}$ for mean atomic weight $0.61m_H$ appropriate for a fully ionized plasma with $n_{\rm He}/n_{\rm H} = 0.1$ by number. The fact that these two raidii are similar is a consequence of the chosen gas temperature and stellar velocity dispersion, which are expected to be in near equilibrium.

2.3. Virial Radius

In standard cosmological terminology, the virial radius, $R_{\rm vir}$, is defined such that the mean density of a halo of mass M_h equals the "virial overdensity" (variously denoted as $\Delta_{\rm vir}$ or Δ_c) times the mean density of the universe. Unfortunately, some confusion has arisen in the proper value of $\Delta_{\rm vir}$, much of it over convention: whether the overdensity is expressed relative to the critical (closure) density, $\rho_{\rm cr} = (3H_0^2/8\pi G)$, or to the matter density, $\rho_m = \Omega_m \rho_{\rm cr}$. Both conventions are used in the literature, but if one is not careful in using a consistent definition of $\Delta_{\rm vir}$, the estimated virial radius will be too small by a factor $\Omega_m^{1/3} \approx 0.67$ and the mean matter density of the halo too large by $\Omega_m^{-1} \approx 3.3$. There are other misapplications of the virial radius because the initial collapse to dynamical equilibrium occurred in the past, when ρ_m was higher, followed by additional infall during galaxy assembly. For these reasons, we develop a physically motivated definition of $R_{\rm vir}(M_h, z, z_a)$ for a halo of mass M_h, observed at redshift z but assembled at an earlier epoch, $z_a > z$. The redshift of halo assembly z_a is taken as the epoch of major virialization ($z_{\rm vir}$) when half the halo mass had collapsed, a useful convention introduced by Tacchella, Trenti, & Carillo (2013) hereafter denoted TTC13.

The basic concept of virialization follows from the assumption of conservation of kinetic energy and potential energy during collapse ($T + W$ = constant) together with the virial theorem ($2T = -W$). The gravitating system is assumed to collapse to half its turnaround radius at twice the turnaround time for cycloidal collapse. The collapsed system has then increased in mean density by a factor of 8 since turnaround. In an Einstein-deSitter universe ($\Omega_0 = 1$), the expanding background density, $\bar{\rho}(t) \propto t^{-2}$, has dropped by a factor of 4 for an expansion parameter $a(t) \propto t^{2/3}$. Thus, one obtains the classic virial overdensity, $\bar{\rho}_{\rm vir} = 32\bar{\rho}_{\rm turn} = (18\pi^2)\bar{\rho}$, where $\bar{\rho}_{\rm turn}$ and $\bar{\rho}_{\rm vir}$ are evaluated at the times of turnaround and virialization, respectively. Cole & Lacey (1996) explored the structure of halos in N-body simulations of clustering in an $\Omega_0 = 1$ universe. They found that the radius, r_{178} enclosing a mean overdensity of 178, accurately separated the virialized halo interior, in approximate dynamic equilibrium, from the exterior where matter was still falling in. This property was noted by Binney & Tremaine (2008), who recommended using $\Delta_{\rm vir} = 200$.

The situation changes in a flat ΛCDM cosmology ($\Omega_m + \Omega_\Lambda = 1$) where both the expanding background and collapse dynamics differ from the $\Omega_0 = 1$ case. Eke et al. (1996) studied virialization dynamics for flat models with $\Omega_m < 1$, but they defined overdensity relative to *closure* density. For values of $\Omega_m \approx 0.3$ at $z \approx 0$, they found $\Delta_c \equiv \bar{\rho}_{\rm vir}/\rho_{\rm cr} \approx 100$. In Figure 1 of their paper, they plotted the dependence of Δ_c on Ω_m, which serves as a proxy for higher redshift, since $\Omega_m(z)$ approaches 1 at the higher redshifts when most systems collapsed. Bryan & Norman (1998) provided an approximate fit, $\Delta_{\rm vir}(z) = [18\pi^2 + 82x - 39x^2]$

where $x = (\Omega_m - 1)$. This expression must be divided by $\Omega_m(z)$ to be consistent with the convention that overdensity is relative to *matter* density. We define $R_{\rm vir}$ through the relation $M_h = (4\pi R_{\rm vir}^3/3)\Delta_{\rm vir}(z_{\rm vir})\bar{\rho}_m(z_{\rm vir})$, where the mean matter density at the virialization (or assembly) redshift is $\bar{\rho}_m(z_{\rm vir}) = \Omega_{m,0}(1+z_{\rm vir})^3\rho_{\rm cr,0}$, and the parameters $\Omega_{m,0}$ and $\rho_{\rm cr,0}$ are defined at the current epoch ($z = 0$). Further discussion is given by Klypin et al. (2011) and van der Marel et al. (2012), both of whom follow the convention that $\Delta_{\rm vir}$ is relative to the mean *matter* density. Their expressions are scaled to a product, $\Omega_m\,\Delta_{\rm vir} \approx 97.2$, evaluated at $z = 0$ for which $\Delta_{\rm vir} = 360$ and $\Omega_{m,0} = 0.27$.

However, many papers in the literature do not account for the fact that virial collapse occurred at earlier times, at redshift $z_{\rm vir}$ when $\Omega_m(z) > \Omega_{m,0}$. For a flat ΛCDM universe with $\Omega_{m,0} = 0.27 - 0.30$ at $z \approx 0$, one finds $\Delta_{\rm vir} \approx 350 \pm 10$ (relative to ρ_m) and a product $\Omega_m\Delta_{\rm vir} \approx 100$. For the more typical collapse at higher redshifts, the product $\Omega_m\,\Delta_{\rm vir} \approx 200$, appropriate for the decrease in $\Delta_{\rm vir}(z)$ as $\Omega_m(z) \to 1$. This overdensity of 200 is slightly above the classical value $\Delta_{\rm vir} \approx 178$ for dynamical reasons discussed by Binney & Tremaine (2008). Consider a galaxy observed at redshift z, associated with halo mass $M_h = (10^{12}M_\odot)M_{12}$ and assembled (at z_a) with half its current mass. The virialization redshift $z_{\rm vir}$ is taken to be z_a, determined from standard cosmological collapse criteria (Lacey & Cole 1993; Sheth & Tormen 1999) and computed as in Trenti, Perna, & Tacchella (2013). Table 2 lists the assembly redshifts, which range from $z_a \approx 1.35$ (at $M_h = 10^{11}\ M_\odot$) to $z_a \approx 0.81$ (at $M_h = 10^{14}\ M_\odot$) for various galaxies observed at $z \approx 0.2 - 0.3$ with stellar masses M_*. Based on these new criteria for galaxy collapse and assembly, the virial radius is:

$$R_{\rm vir}(M_h, z_a) = (206\ {\rm kpc})\, h_{70}^{-2/3}\, M_{12}^{1/3} \left[\frac{\Omega_m(z_{\rm a})\,\Delta_{\rm vir}(z_{\rm a})}{200}\right]^{-1/3} (1+z_a)^{-1}\ . \qquad (12)$$

This expression differs from often-used formulae by the over-density scaling and by the factor $(1+z_{\rm a})^{-1}$, reflecting the fact that most galaxies underwent virialization in the past, not at $z = 0$. After this initial (half-mass) assembly, their proper size changes gradually because of continued mass infall into the halo. To lowest order, this slight growth in $R_{\rm vir}$ ($2^{1/3} \approx 1.26$) is captured in Eq. (12) by using the *current* halo mass (M_h). Second-order effects of late infall or adiabatic compression may occur in the radial mass distribution, which in the NFW formalism changes the scale parameter r_s and concentration c. Some of the infalling matter may not attain virial equilibrium, as the orbital timescale is quite long, $t_{\rm orb} = 2\pi R_{\rm vir}^{3/2}/(GM_h)^{1/2} \approx (8.64\ {\rm Gyr})(1+z_a)^{-3/2}$. This formalism assumes spherical infall and a constant density profile; both approximations change in more realistic collapse scenarios. For example, after accounting for central condensation of the collapsed structure, Rubin & Loeb (2013) find a reduced virial overdensity.

2.4. Escaping Stars Injected into the Halo

In addition to infall, galaxy halos can be probed by fast stars injected radially outward. We therefore discuss the radius at which the fastest galactic stars reach maximum apogalactic distance in a dark matter halo potential. As a simple model that illustrates the basic effect, we assume an isothermal sphere distribution in density, $\rho(r) = (\sigma^2/2\pi G r^2)$ and enclosed mass, $M(r) = (2\sigma^2/G)r$ leading to a constant circular velocity $V_c^2 = GM(r)/r = 2\sigma^2$. For this density and mass distribution, the equation of motion is $\ddot{r} = -GM(r)/r^2$, for a star launched with radial velocity $\dot{r} = v_0$ from radius $r = r_0$, leading to the first integral,

$$\frac{1}{2}\left[v^2 - v_0^2\right] = -(2\sigma^2)\ln(r/r_0)\ . \tag{13}$$

If the star coasts to rest ($v = 0$ at $r = r_{\rm max}$) one has $v_0^2 = 4\sigma^2 \ln(r_{\rm max}/r_0)$ and thus

$$r_{\rm max} = r_0 \exp\left[(v_0/2\sigma)^2\right]\ . \tag{14}$$

Equation (14) illustrates the sensitivity of $r_{\rm max}$ to launching conditions (v_0 and r_0) and halo mass (velocity dispersion σ). For example, a star with $v_0 = 500$ km s^{-1} injected radially from $r_0 = 8.3$ kpc into a halo with $\sigma = 200$ km s^{-1} would have a maximum extent of just 40 kpc. The stellar ejection distance doubles ($r_{\rm max} \approx 79$ kpc) if the launch velocity $v_0 = 600$ km s^{-1}. These distances are not surprising for velocities comparable to the escape speed from the solar circle within the Milky Way ($r_0 = 8.28$ kpc), recently estimated from RAVE stellar survey data to be $V_{\rm esc} = 533^{+54}_{-41}$ km s^{-1} (Piffl et al. 2014).

Repeating the above calculation for the maximum radius in an NFW mass distribution and potential (Equations 3, 4, 5) we find,

$$v_0^2 = \left(\frac{GM_{\rm vir}}{R_{\rm vir}}\right)\frac{2c}{\left[\ln(1+c) - \frac{c}{1+c}\right]}\left[\frac{\ln\left(1 + r_0/r_s\right)}{r_0/r_s} - \frac{\ln\left(1 + r_{\rm max}/r_s\right)}{r_{\rm max}/r_s}\right]\ . \tag{15}$$

This equation can be solved for the velocity v_0 required for a star to reach radius $r_{\rm max}$ from initial radius r_0. Combined with equation (7) for the maximum circular velocity, $V_{\rm max}$, in an NFW halo, we can write the velocity v_0 needed to escape to $r \to \infty$ as

$$v_0 = V_{\rm max}\left[\frac{2}{0.2162}\ \frac{\ln\left(1 + r_0/r_s\right)}{(r_0/r_s)}\right]^{1/2}\ , \tag{16}$$

independent of c. If we take $r_0 = 2.1626\, r_s$ as the radius at $V_{\rm max}$, we find $v_0 = 2.219 V_{\rm max}$. This agrees reasonably well with the Milky Way values, if we assume $V_{\rm max} \approx 240$ km s^{-1} and obtain an escape velocity $v_0 \approx 533$ km s^{-1}.

A related size estimate comes from the radius, $r_{\rm flat}$, to which one must extend an isothermal density distribution to maintain a constant (flat) circular velocity (Smith et al. 2007),

$$r_{\rm flat} = r_0 \exp\left[\frac{V_{\rm esc}^2}{2V_{\rm c}^2} - 1\right] \ . \tag{17}$$

For $V_{\rm esc} = 533^{+54}_{-41}$ km s^{-1} and $V_{\rm c} = 220$ km s^{-1}, one finds a truncation radius $r_{\rm flat} \approx 60$ kpc for $r_0 = 8.3$ kpc, with a large range (40 to 110 kpc) arising from uncertainties in determining $V_{\rm esc}$ and V_c. At larger radii, the circular velocity, $V_c(r)$ likely declines, particularly if the halo density distribution falls off as r^{-3} as in the NFW model. The total (virial) masses of galaxies include substantial mass beyond 50-80 kpc, particularly for halos with $c \geq 10$. Extra mass accretion may account for the discrepancy between low and high values for the Milky Way mass estimates. It is also consistent with the physically motivated revision to the method in which the virial radius is calculated at the "galaxy assembly time" at redshift $z_a > z$ (Section 2.3). We return to these observational issues in Section 3.4.

With the current state of observations, these kinematic constraints suggest halo sizes of 150-200 kpc for L^* galaxies. Future observations of rotation curves, $V_c(r)$, and more distant kinematic tracers (blue horizontal branch stars, hypervelocity stars, globular clusters, and satellites) will be of great help. The RAVE survey data will be greatly improved by the *Gaia* mission, leading to better determinations of escape velocity from the solar circle, and later with LSST, through studies of galaxy satellites, BHB stars, and RR-Lyrae stars.

3. OBSERVATIONS OF GALAXY EXTENTS

3.1. The Milky Way and Andromeda System

Despite their proximity, the Milky Way (MW) and Andromeda (M31) galaxies remain surprisingly uncertain in their inferred mass and extent. Recent MW mass estimates range from just under 10^{12} $M_\odot$ (Smith et al. 2007; Xue et al. 2008; Gnedin et al. 2010; Deason et al. 2012) to more recent values between $(1.2 - 2.0) \times 10^{12}$ $M_\odot$. Some of the lower masses are inferred for stellar tracer distances well within $R_{\rm vir}$. For example, Gnedin et al. (2010) use hypervelocity stars at distances beyond 25 kpc to find $M(\leq 80 \text{ kpc}) = 6.9^{+3.0}_{-1.2} \times 10^{11}$ $M_\odot$. Xue et al. (2008) use 2400 blue horizontal branch stars to estimate $M(\leq 60 \text{ kpc}) = (4.0 \pm 0.7) \times 10^{11}$ $M_\odot$, but they extrapolate to find a virial mass $M_{\rm vir} = (1.0 - 1.2) \times 10^{12}$ $M_\odot$ for two models of the circular velocity curve. Busha et al. (2011) use LMC and SMC kinematics to infer $M_{\rm MW} = (1.2^{+0.7}_{-0.4}) \times 10^{12}$ $M_\odot$.

Boylan-Kolchin et al. (2013) provide a thorough discussion of the previous MW mass measurements, both large and small, but they base their mass on the high probability that

the Leo I satellite is gravitationally bound. For a Leo I distance ($D = 261 \pm 13$ kpc) and Galactocentric space velocity (200 km s^{-1}), they infer a median virial mass $M_{\rm MW} = (1.6^{+0.8}_{-0.6}) \times 10^{12}\ M_\odot$ at 90% confidence. Piffl et al. (2014) use the inferred escape speed at the solar circle, 533^{+54}_{-41} km s^{-1} from the RAVE survey, to estimate $M_{\rm MW} = (1.6^{+0.5}_{-0.4}) \times 10^{12}\ M_\odot$. Watkins et al. (2010) find $M_{\rm MW} = (1.4 \pm 0.3) \times 10^{12}\ M_\odot$ within 300 kpc from 26 satellite galaxies, and McMillan (2011) proposes a mass model with $M_{\rm vir} = (1.26 \pm 0.24) \times 10^{12}\ M_\odot$. Based on the recent dynamical estimates out to larger distances, we conclude that the Milky Way virial mass is likely close to $1.6 \times 10^{12}\ M_\odot$.

Mass estimates for the Andromeda (M31) galaxy include $(1.4 \pm 0.4) \times 10^{12}\ M_\odot$ within 300 kpc from 23 satellite galaxies (Watkins et al. 2010) and $(1.2-1.5) \times 10^{12}\ M_\odot$ within 200 kpc from kinematics of 53 globular clusters (Veljanoski et al. 2013). Tamm et al. (2012) used photometry and the M31 rotation curve, together with several mass distributions, to find a dark-matter halo mass $M_{200} = (0.8-1.1) \times 10^{12}\ M_\odot$, stellar mass $M_* = (1.0-1.5) \times 10^{11}\ M_\odot$, and virial radius 189-213 kpc. Fardal et al. (2013) used Bayesian simulation models of the giant southern stream around Andromeda to derive $\log(M_{\rm M31}/M_\odot) = 12.3 \pm 0.1$. They note that this mass, and those recently inferred for the Milky Way, alleviate the tension between virial mass estimates and the Local Group timing mass, recently estimated at $(4.93 \pm 1.63) \times 10^{12}\ M_\odot$ (van der Marel et al. 2012). Because both the Milky Way and Andromeda halos have likely accreted substantial mass beyond their observable radii (60-80 kpc), their virial masses are taken here to be $M_{\rm MW} = (1.6 \pm 0.4) \times 10^{12}\ M_\odot$ and $M_{\rm M31} = (1.8 \pm 0.5) \times 10^{12}\ M_\odot$, with a sum, $(3.4 \pm 0.6) \times 10^{12}\ M_\odot$, close to the inferred timing mass of the Local Group. Simulations suggest that the remaining mass may consist of "diffuse dark matter" produced by the destruction of sub-halos (Gao et al. 2004). Cosmic scatter could reduce the Local Group mass from the value above, as has been suggested by van der Marel et al. (2012) and Gonzalez, Kravtsov, & Gnedin (2013).

Another measure of gravitational influence is from tidal effects between nearby galaxies. We define the characteristic tidal distance in terms of masses and densities of the two galaxies, treated as deformable fluid spheres (Chandrasekhar 1963) of masses (M_M, M_m) and radii (R_M, R_m),

$$d_{\rm tide} = 2.44 \left(\frac{\rho_M}{\rho_m}\right)^{1/3} R_M = 2.44 \left(\frac{M_M}{M_m}\right)^{1/3} R_m\ . \tag{18}$$

In the case of the Milky Way (MW) and Andromeda (M31) system, internal tidal influences are seen in the form of large-scale streams of stars (Fardal et al. 2013; Ibata et al. 2014), but no obvious tails or bridges produced by external tides are detected. Ibata et al. (2014) find a smooth stellar-light halo in M31 out to 150 kpc, with internal streams from tidally stripped satellites. Usually the Roche formula is applied to situations with $M_M \gg M_m$. However, in the case of the MW-M31 system, we assume $M_M \approx M_m$ to estimate that $d_{\rm tide} \approx 2.44 R_M$

for each galaxy. Here, R_M can be regarded as the effective radius of either galaxy, each of mass $(1-2)\times10^{12}\ M_\odot$. If the distance between the two galaxy centers is $D = 770 \pm 40$ kpc (van der Marel et al. 2012), the absence of strong mutual tidal effects limits their tidal radius to $d_{\rm tide} < D/2$. Equation (18) then implies that most of the stellar and gaseous matter in the two galaxies is confined within radius $R_M < (D/2)/2.44 \approx 160$ kpc. The fluid approximations in making this estimate are large, and more accurate, time-dependent models and searches for external tidal effects would be helpful to set a better limit.

3.2. Gaseous Outflows

Many galaxies undergoing active star formation have been spectroscopically observed at $1.4 \le z \le 2.5$ (Steidel et al. 2004) to have large-scale outflows with bulk velocities of 200-300 km s^{-1}. For a sample of over 200 star-forming galaxies at redshifts $0.4 < z < 1.4$, blueshifted Fe II absorption at greater than 100 km s^{-1} is seen toward 20% of the population (Martin et al. 2012). Because the outflows are collimated, the "outflow fraction" must be signiifcantly higher than the "blueshifted fraction". Some 2.5% have velocities greater than 200 km s^{-1}, with the largest doppler components suggesting velocities up to 500 km s^{-1}. The outflow fraction depends on the observed star-formation rate (SFR) and is three times higher for galaxies with SFR $\approx 20-100\ M_\odot$ yr^{-1} compared to those at $1-10\ M_\odot$ yr^{-1}. If these outflows persist at the observed rates for ~ 1 Gyr, as Martin et al. (2012) suggest, they could remove a large mass of baryons, up to $10^{10}\ M_\odot$. Such metal-enriched outflows could be responsible for the large baryon reservoirs of gas and metals around star-forming galaxies observed in O VI absorption as part of the COS-Halos project. Tumlinson et al. (2011, 2013) found substantial O VI column densities, $N_{\rm OVI} \ge 10^{14.3}$ cm^{-2} out to distances of 100-150 kpc, toward a sub-sample of 28 galaxies with active star formation. These O VI-bearing halos surround galaxies with SFRs of $1-10\ M_\odot$ yr^{-1} and specific SFRs greater than 10^{-11} yr^{-1}.

How far will these galactic winds expand before stalling? Several simulations (Furlanetto & Loeb 2003; Oppenheimer & Davé 2008) estimate that these outflows expand to ~ 100 kpc, distances inferred observationally in metal-line auto-correlation of C IV absorbers (Martin et al. 2010). A simple estimate illustrates the main effects, as winds encounter surrounding gas in the CGM and produce a "galactopause" where the wind ram pressure, $P_w = \rho_w V_w^2 = (\dot{M}_w V_w/\Omega_w r^2)$, equals the confining gas pressure of the CGM, $P_{\rm CGM} = n_{\rm tot}\, kT = 2.17 n_H k T_{\rm CGM}$. Here, $\dot{M}_w = \Omega_w r^2 \rho_w V_w$ is the mass-loss rate of a conical outflow into total solid angle Ω_w, ρ_w is the mass density, and V_w is the wind velocity. Observers and modelers typically relate $\dot{M}_w$ to the SFR through a "mass-loading factor", defined here as $\beta_m = \dot{M}_w/{\rm SFR}$. This mass loading has been inferred from optical and X-ray

data to lie in the range $\beta_m = 1 - 3$ (Strickland & Heckman 2009). In a careful study of the dwarf starburst galaxy NGC 1569, Martin, Kobulnicky, & Heckman (2002) use observations of the SFR, Hα emission, metallicities, and X-ray emission from the outflow to estimate $M_X/M_{\rm ejecta} \approx 6 - 36$ for the mass ratio of X-ray emitting wind to stellar ejecta. With standard assumptions about the ratio of ejecta mass to star formation, this range corresponds to mass loading factors $\beta_m \approx 1 - 6$.

For the CGM gas pressure in low-redshift, actively star-forming galaxies, we use the observed O VI column densities ($10^{14.5}$ cm^{-2}) and spatial impact parameters (100-150 kpc) from COS-Halos data, which suggest total hydrogen column densities $N_H \approx (5 - 10) \times 10^{18}$ cm^{-2} for solar oxygen abundances, (O/H) $\approx 5 \times 10^{-4}$, and O VI ionization fractions $f_{\rm OVI} \approx 0.1 - 0.2$. Stocke et al. (2013) estimated a mean pressure $\langle P/k \rangle \approx 10$ cm^{-3} K (with a range from 3 to 60 cm^{-3} K) for warm clouds in the CGM of low-redshift galaxies. Using O VII X-ray absorption through the Galactic halo, Miller & Bregman (2013) modeled thermal pressures $P/k \approx [41, 24]$ cm^{-3} K for halos with characteristic scales of [50, 100] kpc and gas temperature $\log T = 6.1$.

Thus, in the inner portions of the CGM that would initially confine the outflows, the gas pressure is scaled to $P_{\rm CGM}/k = 2.17 n_H T = (40$ cm^{-3} K$) P_{40}$, appropriate for hydrogen number density $n_H \approx 10^{-5}$ cm^{-3}, halo virial temperature $T_{\rm CGM} \approx 2 \times 10^6$ K, and fully ionized gas with He/H = 0.0833 by number. For wind speeds $V_w = (200$ km s$^{-1}) V_{200}$, the approximate radius of the galactopause is

$$R_{\rm wind} = \left(\frac{\dot{M}_w V_w}{\Omega_w P_{\rm CGM}} \right)^{1/2} = (140 \text{ kpc}) \left(\frac{\rm SFR}{10 \ M_\odot \ {\rm yr}^{-1}} \right)^{1/2} \left(\frac{\Omega_w}{4\pi} \right)^{-1/2} \left(\frac{\beta_m \, V_{200}}{P_{40}} \right)^{1/2} . \quad (19)$$

The combination of parameters ($\beta_m \, V_{200}/P_{40}$) is expected to be of order unity, while bipolar wind solid angles Ω_w typically cover 10-40% of 4π sterradians for starburst galaxies (Veilleux, Cecil, & Bland-Hawthorn 2005). If the galaxy wind breaks through the higher-density CGM, the IGM pressure will be considerably lower, and the metal-enriched winds will expand well beyond 200 kpc, depending on the duration of the starburst outflow. Simulations of the low-redshift IGM (e.g., Smith et al. 2011) find a wide range of intergalactic gas pressures in the Lyα forest ($P/k \approx 0.1 - 2$ cm^{-3} K) and hotter O VI-bearing gas ($P/k \approx 3 - 30$ cm^{-3} K).

In the above estimate, the star-formation rates were scaled to 10 $M_\odot$ yr^{-1}. In the sample of active star-forming galaxies at $z \sim 1$ (Martin et al. 2012), the observed SFRs range from 20-100 $M_\odot$ yr^{-1}, while in the sample of 28 active COS-Halos galaxies at $z \approx 0.15 - 0.35$ (Tumlinson et al. 2013) the SFRs are 1–10 $M_\odot$ yr^{-1}. These rates likely reflect the general decline in SFR history among all galaxies, from $z = 1 - 2$ to the present epoch.

3.3. Local Environment: Intervening Absorbers and Galaxies

Indirect estimates of the sizes of extended gaseous halos and metal-enriched outflows around galaxies can be made from observations of QSO absorption lines. In a pioneering paper, Bahcall & Spitzer (1969) proposed that these absorbers are produced in "extended halos of normal galaxies" and used the line frequency, $d\mathcal{N}/dz$, the number of absorbers per unit redshift, to constrain the halo cross section. Their estimate, $R_0 \approx 100$ kpc, for the radius of a spherical halo is comparable to recent estimates from UV spectra of low-redshift QSO absorbers obtained from HST (Shull et al. 1996; Stocke et al. 2006; Prochaska et al. 2011). Those UV studies related line frequency of absorbers in H I (Lyα) or the O VI doublet (1032, 1038 Å) to the absorber cross section and space density, $\phi_{\rm gal}$, of galaxies, using a luminosity function to extrapolate to dwarf galaxy scales. At redshifts $z \leq 0.4$ and ignoring cosmological effects, the number of of O VI absorbers per unit redshift is $d\mathcal{N}/dz \approx (c/H_0)(\pi R_0^2)\phi_{\rm gal}$, from which one infers an absorber size

$$R_0 = \left[\frac{d\mathcal{N}/dz}{(c/H_0)\,\pi\,\phi_{\rm gal}}\right]^{1/2} \approx (157\ {\rm kpc}) \left[\frac{d\mathcal{N}/dz}{20}\right]^{1/2} \left[\frac{\phi_{\rm gal}}{0.06\ {\rm Mpc}^{-3}}\right]^{-1/2} . \qquad (20)$$

This formula uses the observed $d\mathcal{N}/dz \approx 20$ down to 10 mÅ equivalent width for the O VI 1032 Å absorption line in low-redshift absorber surveys (Danforth & Shull 2008; Tilton et al. 2012). We adopt a Hubble constant $H_0 = (70\ {\rm km\ s^{-1}\ Mpc^{-1}})h_{70}$, a Hubble length $(c/H_0) = (4286\ {\rm Mpc})\,h_{70}^{-1}$, and a galaxy luminosity function,

$$\phi(L)\,dL = \frac{\phi_*}{L^*}\left(\frac{L}{L^*}\right)^{\alpha} \exp(-L/L^*)\,dL\ , \qquad (21)$$

with normalization $\phi_* = (6.07 \pm 0.51) \times 10^{-3}\,h_{70}^3\ {\rm Mpc}^{-3}$ at B-band absolute magnitude $M^* = -20.37 \pm 0.04$ and faint-end slope $\alpha \approx -1.13 \pm 0.02$ given by the Millennium galaxy catalog (Driver et al. 2005) and converted to $h_{70} = 1$ scale. The galaxy space density is scaled to 0.06 Mpc^{-3}, a value appropriate for extrapolation of $\phi(L)$ down to dwarf galaxies of luminosity $L \geq 0.1L^*$, which have ~ 10 times the space density of galaxies with $L \geq L^*$ for $\alpha = -1.1 \pm 0.1$. These sizes are consistent with surveys that attempt to match the nearest-neighbor galaxy, in 3D space, to low-redshift absorbers (Stocke et al. 2006, 2013). The galaxy spatial distributions in the surveys suggest that the nearest galaxies to O VI absorbers lie at distances ~ 1 Mpc from an L^* galaxy and at ~ 200 kpc from a galaxy at $0.1L^*$.

3.4. Halo Masses and Virial Radii from Galaxy Abundance Matching

Observers often lack direct measurements of galaxy masses. Instead, they estimate halo mass, $M_{\rm h}$, from the inferred stellar mass M_* or galaxy luminosity L, using the technique of "abundance matching" (Behroozi et al. 2010; Moster et al. 2010, 2013). By matching the abundance of dark-matter halos in simulations to observed galaxy distributions in stellar mass and luminosity, they attempt to characterize the relationship between the stellar masses of galaxies and the masses of the dark matter halos in which they live. Moster et al. (2010) obtain a parameterized stellar-to-halo mass relation by populating halos and subhalos in an N-body simulation with galaxies and requiring that the observed stellar mass function be reproduced. In a different approach, Tacchella, Trenti, & Carollo (TTC13) assume that the rest-frame UV luminosity and stellar mass of a galaxy are related to its dark-matter halo assembly and gas infall rate. Galaxies are assumed to experience a burst of star formation at the halo assembly time (redshift $z = z_a$) followed by a constant star formation rate sustained by steady gas accretion that provides the dominant contribution to the UV luminosity at all redshifts. The model is calibrated by constructing a galaxy luminosity versus halo mass relation at $z = 4$ via abundance matching. After this luminosity calibration, the model naturally fits the $z = 4$ stellar mass function and correctly predicts the evolution of both luminosity and stellar mass functions from $z \approx 8$ to $z \approx 0$.

Generically, halo-matching methods have many similarities, including the flattening at high M_* of the relation that maps stellar mass M_* into halo mass M_h. The similar relation between luminosity L of the central galaxy and the dark-matter halo has been explained (Cooray & Milosavljevic 2005) as the result of a decline in merging efficiency for the accretion of satellites. Flattening of the M_* curve at high M_h predicts that ($z \approx 0$) galaxies with $M_* > 10^{11}\ M_\odot$ reside in very massive halos, $M_h > 10^{13}\ M_\odot$, although errors in M_* (or L) can create large uncertainties in the inferred M_h. A more subtle effect is that scatter in M_* is amplified asymmetrically in M_h; simply adopting the mean relation for $M_h(M_*)$ leads to errors (Behroozi et al. 2010). Various halo-matching methods differ in specific details, including the redshift evolution of the ratio M_*/M_h. Here, we adopt the TTC13 formalism, which has a clear physical basis for mass assembly and rest-frame UV luminosity evolution.

The COS-Halos study (Tumlinson et al. 2013; Werk et al. 2013) used the Moster et al. (2010) technique, whereas this paper adopts the TTC13 formalism. Both methods find that galaxies with $L > L^*$ correspond to large halo masses. However, as seen in Table 3, there are differences between the two methods in the estimated halo masses and virial radii of the 44 galaxies in the COS-Halos sample. The inferred values of M_h and $R_{\rm vir}$ are particularly uncertain for galaxies with $L > L^*$. Comparing values in Columns (5)–(8), one sees that the new method gives virial radii smaller by factors 0.4-0.8. Statistically, the ratio of mean virial

radii computed with the two methods is $\langle R_{\rm vir}^{\rm (new)}\rangle/\langle R_{\rm vir}^{\rm (old)}\rangle = 0.63 \pm 0.04$, with the largest change occurring for lower-mass halos, $\log M_* = 10.0 - 10.4$ (all masses are expressed in $M_\odot$ units). Table 4 summarizes the statistical differences for the 44 galaxies in this sample, including subsets of galaxies at low, moderate, and high stellar masses.

This decrease in $R_{\rm vir}$ occurs primarily because we evaluate the galaxy collapse and virialization at overdensity, $\Delta_{\rm vir}$, at the redshifts of galaxy assembly, $z_a \approx 0.74 - 1.29$, rather than at the observed redshifts $z \approx 0.2 - 0.3$. In addition, the conversion from M_* to M_h using modeling or abundance matching differs between methods, particularly in its dependence on redshift. Another difference is that we define $\Delta_{\rm vir}$, relative to the *matter* density rather than the *critical* density. In a few instances with $L > L^*$ and large stellar masses, $\log M_* \geq 11.3$, we find large virial radii, $R_{\rm vir} > 400$ kpc, and anomalously large massive halos, $\log M_h > 13.8$. This result occurs because halo-matching algorithms and simulated luminosity functions find large stellar masses to be rare and associate them with very massive halos. Applied to the large Local Group galaxies, halo-matching gives high values for the Milky Way ($\log M_h = 12.55^{+0.18}_{-0.16}$ and $R_{\rm vir} = 153^{+25}_{-16}$ kpc for $\log M_* = 10.7 \pm 0.1$) and M31 ($\log M_h = 13.35^{+0.24}_{-0.22}$ and $R_{\rm vir} = 303^{+69}_{-52}$ kpc for $\log M_* = 11.1 \pm 0.1$). Unfortunately for CGM studies, halo-matching for $L > L^*$ (high M_*) galaxies remains an uncertain technique, as demonstrated in Figure 1 of Stocke et al. (2013).

4. CONCLUSIONS AND DISCUSSION

This paper reviews current observations and inferences about the spatial extent of galaxies, and the extent of their gravitational influence. These included several dynamical measures: the "gravitational radius" $r_g = GM^2/|W|$, the "radius of influence" $R_{\rm infl} = GM/\sigma_\parallel^2$, and the "accretion radius" $R_{\rm accr} = 2GM/c_s^2$. Clearly, these definitions are related for systems near dynamical equilibrium in the gravitational potential of the galactic halo. For example, in Section 2.1 and Table 1, we found a ratio $r_g/R_{\rm vir} = 0.54 - 0.69$ for NFW halos with concentrations ranging from $c = 20$ to $c = 5$. Various estimates of radial extent from rotation curves and injection of fast stars into extended halos suggest 150-200 kpc extents for halo masses of 10^{12} $M_\odot$. Kinematic observations of the Milky Way and M31 give masses $\sim 10^{12}$ $M_\odot$ within 60-80 kpc. For Galactic escape velocity $V_{\rm esc} = 533^{+54}_{-41}$ km s^{-1}, these distances are comparable to the radius, 60^{+50}_{-20} kpc, to which one would need to extend an isothermal-sphere distribution, with $M(r) \propto r$, and maintain a rotation curve with constant circular velocity $V_c = 220$ km s^{-1}. Somewhat larger halo masses, $\log M_{\rm MW} = 12.2 \pm 0.1$ and $\log M_{\rm M31} = 12.3 \pm 0.1$ (all masses in $M_\odot$ units) have been inferred for the Milky Way and M31 out to larger radii, using globular clusters, satellite galaxies, and stellar streams.

Their mass sum, $\log M \approx 12.55 \pm 0.14$, is comparable to recent estimates of the timing mass of the Local Group, $\log M_{\rm LG} = 12.69^{+0.13}_{-0.19}$ (van der Marel 2012), although a recent study (Gonzalez et al. 2013) used cosmological simulations of halo pairs and a likelihood correction to find a lower value, $\log M_{\rm LG} = 12.38^{+0.09}_{-0.07}$. For either of these masses, the Milky Way and Andromeda are likely to have radial extents ~ 200 kpc.

The answer to the question posed in the title to this paper depends on how one wishes to define or observe the "edge of a galaxy". Does a galaxy end because of gravity or outflows? This paper suggests that the best definition of $R_{\rm vir}$ is in terms of gravitational binding. Dark matter halos have very large extents, but galactic outflows can drive gas out of the stellar disk, into the (bound) halo, and often into the (unbound) CGM and IGM. We have formulated a new definition of virial radius in this spirit, based on galaxy assembly in the past, when the background density was higher. As a result, we find virial radii smaller by factors of 0.5-0.6, with important consequences for assessing whether the extended absorption seen with COS is bound halo gas, or unbound gas on its way to the IGM.

The main conclusions of this paper are as follows:

- A revised formulation of virial radius, $R_{\rm vir}(M_h, z_a)$, expresses the critical overdensity $\Delta_{\rm vir}$ relative to the background matter density, $\bar{\rho}_m(z_a)$, evaluated at z_a, the redshift of galaxy assembly when half the halo mass had collapsed. Here, z_a depends on M_h and is inferred from stellar mass M_*. For dynamical consistency, the circumgalactic medium of large galaxies is defined by their gravitationally bound regions, estimated from the virial radius and related to the gravitational radius, $r_g(M_h, c) \approx (0.54 - 0.69) R_{\rm vir}$, for NFW models with concentrations $c = 5 - 20$.

- For galaxies with halo mass $11.0 \leq \log M_h \leq 14.0$ observed by HST/COS at redshifts $0.14 < z < 0.35$, the assembly redshifts are $1.35 > z_a > 0.81$. Because virialization was largely determined by early collapse, when the background density was higher, we adopt $\Delta_{\rm vir}\Omega_m \approx 200$ and $R_{\rm vir}$ is reduced by a factor $(1 + z_a)$ compared to $z \approx 0$.

- In this new formulation of $R_{\rm vir}$, halo masses are estimated from stellar masses with halo-matching based on a physically motivated model (TTC13) for galaxy assembly consistent with rest-frame UV luminosity functions from $z = 0 - 8$. Applied to 44 COS-Halos galaxies, this formalism yields virial radii smaller by factors of 0.5-0.6 (even less for $\log M_* < 10.4$). Galaxies with $L \approx L^*$ ($\log M_h \approx 12.5$) have $R_{\rm vir} \approx 200$ kpc, consistent with their observed radial extent. A generic feature of halo-matching methods is the flattening of the relation between M_* and M_h (or luminosity L and M_h) leading to anomalously large halo masses ($\log M_h > 13.8$ for $\log M_* > 11.3$) and unrealistically large virial radii ($R_{\rm vir} > 400$ kpc).

- If confined by CGM gas pressure, the wind galactopause is predicted to occur at distances $R_{\rm wind} \approx 100{-}200$ kpc for SFR = 10-30 $M_\odot$ yr^{-1}, mass-loading factors $\beta_m \approx 1{-}3$, and the observed range of CGM gas pressures and wind velocities. Stronger galaxy winds could break out into the lower density IGM, with radial extents beyond 200 kpc determined by the strength, collimation, and duration of the outflow.

- For dynamical masses of the large Local Group galaxies, we adopt: Milky Way ($\log M_h \approx 12.2 \pm 0.1$) and M31 ($\log M_h \approx 12.3 \pm 0.1$) with (gravitational) radial extents of 150-200 kpc. In our new formalism, the Milky Way stellar mass, $\log M_* = 10.7 \pm 0.1$, would correspond to somewhat higher halo mass $\log M_h = 12.55^{+0.18}_{-0.16}$ and virial radiius $R_{\rm vir} = 153^{+25}_{-16}$ kpc for assembly at $z_a = 1.06 \pm 0.03$. The inferred M_h for M31 is anomalously high ($\log M_h = 13.35^{+0.24}_{-0.22}$), which suggests caution in using halo-matching to obtain M_h and $R_{\rm vir}$ for massive, luminous galaxies ($L > L^*$).

As noted earlier, the new definition of $R_{\rm vir}$ is important in deciding whether gas in the vicinity of galaxies is gravitationally bound or unbound. Whether galaxies are "open or closed boxes" helps to determine the metal evolution of galaxies and the extent of metal-pollution of the IGM. It also suggests that astronomers should be careful in making interchangable use of the terms CGM and Halo. Matter in the galactic halo is *gravitationally bound*, while the circumgalactic (gaseous) medium may in fact be *unbound outflows* that will merge into the IGM. What many observers are calling the CGM is probably gas at the CGM–IGM interface.

In observations of large metal-enriched reservoirs around star-forming galaxies (Tumlinson et al. 2013; Stocke et al. 2013), the radial offset distances R of the QSO sight lines were normalized to $R_{\rm vir}$, with much of the metal-enriched gas within $R < R_{\rm vir}$. With the revised (smaller) virial radii (Table 3 and Figure 1) some of this metal-enriched gas extends beyond the region of strong gravitational influence, probably on its way out to the IGM. This trend is seen in the 28 actively star-forming galaxies in the COS-Halos sample, whereas the undetected O VI around 16 passive galaxies all had sight lines with $R < R_{\rm vir}$. In future work, both data sets will be examined carefully with the new formalism.

I thank Crystal Martin, Michele Trenti, Massimo Ricotti, John Stocke, Brian Keeney, Blair Savage, and Vasily Belokurov for helpful discussions, and Evan Tilton and Joshua Moloney for comments on the manuscript. This research was supported by the Astrophysical Theory Program at the University of Colorado Boulder (grant NNX07-AG77G from NASA). I am grateful to the Institute of Astronomy at Cambridge University for their stimulating scientific environment and support through the Sackler Visitor Program.

REFERENCES

Anderson, M. E., & Bregman, J. N. 2010, ApJ, 714, 320

Anderson, M. E., Bregman, J. N., & Dai, X. 2013, ApJ, 762, 106

Bahcall, J. N., & Spitzer, L. 1969, ApJ, 156, L63

Behroozi, P. S., Conroy, C., & Wechsler, R. H. 2010, ApJ, 717, 379

Binney, J., & Tremaine, S. 2008, Galactic Dynamics, (Princeton Univ. Press)

Boylan-Kolchin, M., Bullock, J., Sohn, S. T., Besla, G., & van der Marel, R. 2013, ApJ, 768, 140

Bryan, G. L., & Norman, M. L. 1998, ApJ, 495, 80

Busha, M. T., Wechsler, R., Behroozi, P. S., Gerke, B. F., Klypin, A. A., & Primack, J. R. 2011, ApJ, 743, 40

Cen, R., & Ostriker, J.P. 1999, ApJ, 514, 1

Chandrasekhar, S. 1963, ApJ, 138, 1182

Cole, S., & Lacey, C. 1996, MNRAS, 281, 716

Collins, J. A., Shull, J. M., & Giroux, M. L. 2005, ApJ, 623, 196

Cooray, A., & Milosavljevic, M. 2005, ApJ, 627, L89

Danforth, C. W. & Shull, J. M. 2008, ApJ, 679, 194

Davé, R., Hernquist, L., Katz, N., & Weinberg, D. H. 1999, ApJ, 511, 521

Deason, A. J., Belokurov, V., Evans, N. W., et al. 2012, MNRAS, 425, 2840

Driver, S. P., Liske, J., Cross, N. J. G., De Propris, R., & Allen, P. D. 2005, MNRAS, 360, 81

Eke, V. R., Cole, S., & Frenk, C. S. 1996, MNRAS, 282, 263

Fang, T., McKee, C. F., Canizares, C. R., & Wolfire, M. 2006, ApJ, 644, 174

Fardal, M. A., Weinberg, M. D., Babul, A., et al. 2013, MNRAS, 434, 2779

Ferrarese, L., & Ford, H. 2005, Space Science Reviews, 116, 523

Furlanetto, S. R., & Loeb, A. 2003, ApJ, 588, 18

Gao, L., White, S. D. M., Jenkins, A., Stoehr, F., & Springel, V. 2004, MNRAS, 355, 819

Gnedin, O. Y., Brown, W. R., Geller, M. J., & Kenyon, S. J. 2010, ApJ, 720, L108

Gonzalez, R. E., Kravtsov, A. V., & Gnedin, N. Y. 2013, ApJ, submtted (arXiv:1312.2587)

Gupta, A., Mathur, S., Krongold, Y., Nicastro, F., Galeazzi, M. 2012, ApJ, 756, L8

Hagihara, T., Yao, Y., Yamasaki, N., et al. 2010, PASJ, 62, 723

Hagihara, T., Yamasaki, N., Mitsuda, K., et al. 2011, PASJ, 663, 869

Ibata, R. A., Lewis, G. F., McConnachie, A. W., et al. 2014, ApJ, 780, 128

Klypin, A. A.,Trujillo-Gomez, S., & Primack, J. 2011, ApJ740, 102

Lacey, C., & Cole, S. 1993, MNRAS, 262, 627

Lehner, N., & Howk, J. C. 2011, Science, 334, 955

Martin, C. L., Kobulnicky, H. A., & Heckman, T. M. 2002, ApJ, 574, 663

Martin, C. L., Scannapieco, E., Ellison, S. L., et al. 2010, ApJ, 721, 174

Martin, C. L., Shapley, A. E., Coil, A. L., et al. 2012, ApJ, 760, 127

McKernan, B., Yaqoob, T., & Reynolds, C. S. MNRAS, 361, 1337

McMillan, P. J. 2011, MNRAS, 414, 2446

Miller, M. J., & Bregman, J. N. 2013, ApJ, 770, 118

Moster, B. P., Somerville, R. S., Maulbetsch, C., et al. 2010, ApJ, 710, 903

Moster, B. P., Nash, T., & White, S. D. M. 2013, MNRAS, 428, 3121

Navarro, J., F. Frenk, C. S., & White, S. D. M. 1997, ApJ, 490, 493

Nicastro, F., Zezas, A., Drake, J., et al. 2002, ApJ, 573, 157

Oppenheimer, B., & Dave, R. 2008, MNRAS, 387, 577

Penton, S., Stocke, J. T., & Shull, J. M. 2002, ApJ, 565, 720

Piffl, T., Scannapieco, C., Binney, J., et al. 2014, A&A, in press (arXiv:1309.4293)

Prochaska, J. X., Weiner, B., Chen, H.-W., et al. 2011, ApJ, 740, 91

Rubin, D., & Loeb, A. 2013, JCAP, in press (arXiv:1311.5594)

Rubin, V., Ford, W. K., & Thonnard, N. 1980, ApJ, 238, 471

Rudie, G., Steidel, C. C., Trainor, R. F., et al. 2012, ApJ, 750, 67

Sargent, W. L. W., Young, P. J., Boksenberg, A., & Tytler, D. 1980, ApJS, 42, 41

Sembach, K. R., Wakker, B. P., Savage, B. D., et al. 2003, ApJS, 146, 165

Sheth, R. K., & Tormen, G. 1999, MNRAS, 308, 119

Shull, J. M., Stocke, J. T., & Penton, S. 1996, AJ, 111, 72

Shull, J. M., Jones, J. R., Danforth, C. W., & Collins, J. A. 2009, ApJ, 699, 754

Shull, J. M., Smith, B. D., & Danforth, C. W. 2012, ApJ, 759, 23

Smith, M. C., Ruchti, G. R., Helmi, A., et al. 2007, MNRAS, 379, 755

Smith, B. D., Hallman, E. J., Shull, J. M., & O'Shea, B. W. 2011, ApJ, 731, 6

Spitzer, L. 1956, ApJ, 124, 20

Spitzer, L. 1969, ApJ, 158, L139

Springel, V., White, S. D. M., Jenkins, A., et al. 2005, Nature, 435, 629

Steidel, C. C., Shapley, A. E., Pettini, M., et al. 2004, ApJ, 604, 534

Stocke, J. T., Penton, S. V., Danforth, C. W., Shull, J. M., Tumlinson, J., & McLin, K. M. 2006, ApJ, 641, 217

Stocke, J. T., Keeney, B. A., Danforth, C. W., et al. 2013, ApJ, 763, 148

Strickland, D. K., & Heckman, T. M. 2009, ApJ, 697, 2030

Tacchella, S., Trenti, M., & Carollo, M. 2013, ApJ, 768, L37 (TTC13)

Tamm, A., Tempel, E., Tenjes, P., Tihhonova, O., & Tuvikene, T. 2012, A&A, 546, A4

Tilton, E., Danforth, C. W., Shull, J. M., & Ross, T. L. 2012, ApJ, 759, 112

Trenti, M., Perna, R., & Tacchella, S. 2013, ApJ, 773, L22

Tripp, T. M., Meiring, J. D., Prochaska, J. X., et al. 2011, Science, 334, 952

Tumlinson, J., Thom, C., Werk, J. K., et al. 2011, Science, 334, 948

Tumlinson, J., Thom, C., Werk, J. K., et al. 2013, ApJ, 777, 59

van der Marel, R., P., Fardal, M., Besla, G. et al. 2012, ApJ, 753, 8

Veilleux, S., Cecil, G., & Bland-Hawthorn, J. 2005, ARA&A, 43, 769

Veljanoski, J., Ferguson, A. M. N., Mackey, A. D., et al. 2013, ApJ, 768, L33

Wang, Q. D., Yao, Y., Tripp, T., et al. 2005, ApJ, 635, 386

Watkins, L. L., Evans, N. W., & An, J. H. 2010, MNRAS, 406, 264

Werk, J., Prochaska, J. X., Thom, C., et al. 2012, ApJS, 198, 3

Werk, J., Prochaska, J. X., Thom, C., et al. 2013, ApJS, 204, 17

Xue, X. X., Rix, H.-W., Zhao, G., et al. 2008, ApJ, 684, 1143

Yao, Y., & Wang, Q. D. 2005, ApJ, 624, 751

Table 1. **Gravitational Radius (r_g) for Various Density Models**

Model	Density $\rho(r)$[a]	Scale[a]	r_g[a]
Uniform Sphere	$\rho = \rho_0$ for $r \leq R$	R	$1.67R$
Plummer Model	$(3M/4\pi b^3)[1 + (r/b)^2]^{-5/2}$	b	$3.40b$
Jaffe Model	$\rho_0(r/a)^{-2}(1 + r/a)^{-2}$	a	$2a$
Hernquist Model	$\rho_0(r/a)^{-1}(1 + r/a)^{-3}$	a	$6a$
NFW Model ($c = 5$)	$\rho_0(r/r_s)^{-1}(1 + r/r_s)^{-2}$	r_s	$3.44r_s$
NFW Model ($c = 10$)	$\rho_0(r/r_s)^{-1}(1 + r/r_s)^{-2}$	r_s	$6.41r_s$
NFW Model ($c = 15$)	$\rho_0(r/r_s)^{-1}(1 + r/r_s)^{-2}$	r_s	$8.81r_s$
NFW Model ($c = 20$)	$\rho_0(r/r_s)^{-1}(1 + r/r_s)^{-2}$	r_s	$10.8r_s$

[a]Radial density distribution, characteristic radial scale, and gravitational radius, $r_g = GM^2/|W|$, defined in terms of mass and potential energy of system (Binney & Tremaine 2008). For the NFW density distribution, the total mass diverges logarithmically with radius, but we define r_g for the mass inside $R_{\rm vir} = c\, r_s$ as shown in Equation (9).

Table 2. **Redshifts of Galaxy Halo Assembly (z_a)**

$\log(M_h/M_\odot)$	z_a[a]	$\log(M_h/M_\odot)$	z_a[a]
9.00	1.709	12.25	1.112
9.25	1.666	12.50	1.070
9.50	1.620	12.75	1.026
9.75	1.572	13.00	0.979
10.00	1.531	13.25	0.936
10.25	1.486	13.50	0.891
10.50	1.439	13.75	0.844
10.75	1.394	14.00	0.806
11.00	1.346	14.25	0.765
11.25	1.302	14.50	0.722
11.50	1.255	14.75	0.684
11.75	1.216	15.00	0.645
12.00	1.155		

[a]Halo assembly formalism (TTC13) model) assumes that half the halo mass ($M_h/2$) is assembled at redshift z_a (Trenti, Perna, & Tacchella 2013). Values of z_a are used in virial radius (Equation 12). See Sections 2.3 and 3.4 for discussion and applications.

Table 3. **Masses and Virial Radii of 44 COS-Halos Galaxies**[a]

QSO (Galaxy)[a]	z[a]	(L/L^*)[a]	$\log M_*$[a]	$\log M_h$[b] (old)	$\log M_h$[b] (new)	$R_{\rm vir}$[b] (old)	$R_{\rm vir}$[b] (new)	z_a[b]	R[a]
(1)	(2)	(3)	(4)	(5)	(6)	(7)	(8)	(9)	(10)
J0226+0015(268,22)	0.22744	0.51	10.8	12.62	12.73	303	178	1.03	80
J0401-0540 (67,24)	0.21969	0.37	10.2	12.08	11.86	200	85	1.19	86
J0803+4332(306,20)	0.25347	1.63	11.3	13.48	13.84	581	462	0.83	79
J0910+1014 (34,46)	0.14274	0.60	10.6	12.48	12.39	279	133	1.09	116
J0910+1014(242,34)	0.26412	2.16	11.5	13.76	14.40	716	747	0.74	139
J0914+2823 (41,27)	0.24431	0.37	9.8	11.87	11.48	169	61	1.26	104
J0925+4004(196,22)	0.24745	1.48	11.3	13.45	13.84	569	462	0.83	86
J0928+6025(110,35)	0.15400	0.52	10.8	12.65	12.73	317	178	1.03	94
J0935+0204 (15,28)	0.26228	0.79	11.0	12.88	13.13	365	251	0.95	114
J0943+0531(106,34)	0.22839	0.74	10.8	12.61	12.73	300	178	1.03	125
J0943+0531(216,61)	0.14311	0.72	11.0	12.80	13.13	382	251	0.95	154
J0943+0531(227,19)	0.35295	0.24	9.6	11.66	11.31	141	69	1.29	95
J0950+4831(177,27)	0.21194	1.44	11.2	13.30	13.59	511	371	0.88	94
J1009+0713(204,17)	0.22784	0.28	9.9	11.90	11.56	174	66	1.24	62
J1009+0713(170,9)	0.35569	0.29	10.3	12.06	11.98	189	94	1.16	45
J1016+4706(274,6)	0.25195	0.23	10.2	12.10	11.86	202	85	1.19	24
J1016+4706(359,16)	0.16614	0.44	10.5	12.35	12.24	251	117	1.12	46
J1112+3539(236,14)	0.24670	0.52	10.3	12.17	11.98	214	94	1.16	54
J1133+0327(110,5)	0.23670	1.94	11.2	13.19	13.59	515	371	0.88	14
J1133+0327(164,21)	0.15449	0.19	10.1	12.09	11.76	206	78	1.21	56
J1157-0022(230,7)	0.16378	0.55	10.9	12.72	12.91	334	207	1.00	20
J1220+3853(225,38)	0.27371	0.66	10.8	12.53	12.73	279	178	1.03	159
J1233+4758(94,38)	0.22210	0.70	10.8	12.58	12.73	295	178	1.03	137
J1233-0031(168,7)	0.31850	0.37	10.6	12.30	12.39	230	133	1.09	33
J1241+5721(199,6)	0.20526	0.20	10.2	12.10	11.86	205	85	1.19	21
J1241+5721(208,27)	0.21780	0.20	10.1	12.02	11.76	192	78	1.21	92
J1245+3356(236,36)	0.19248	0.20	9.9	11.81	11.56	178	66	1.24	117
J1322+4645(349,11)	0.21418	0.58	10.8	12.50	12.73	303	178	1.03	39
J1330+2813(289,28)	0.19236	0.24	10.3	12.22	11.98	225	94	1.16	91
J1342-0053(157,10)	0.22702	1.08	11.0	12.67	13.13	345	251	0.95	37
J1342-0053(77,10)	0.20127	0.25	10.5	12.34	12.24	247	117	1.12	34
J1419+4207(132,30)	0.17925	0.55	10.6	12.46	12.39	272	133	1.09	92
J1435+3604(126,21)	0.26226	0.33	10.4	12.20	12.01	218	97	1.15	86
J1435+3604(68,12)	0.20237	1.37	11.1	13.08	13.35	433	302	0.92	40
J1437+5045(317,38)	0.24600	0.46	10.2	12.06	11.86	196	85	1.19	149

Table 3—Continued

QSO (Galaxy)[a]	z[a]	(L/L^*)[a]	$\log M_*$[a]	$\log M_h$[b] (old)	$\log M_h$[b] (new)	$R_{\rm vir}$[b] (old)	$R_{\rm vir}$[b] (new)	z_a[b]	R[a]
(1)	(2)	(3)	(4)	(5)	(6)	(7)	(8)	(9)	(10)
J1445+3428(232,33)	0.21764	0.29	10.4	12.26	12.01	230	97	1.15	117
J1514+3619(287,14)	0.21223	0.18	9.7	11.81	11.39	164	57	1.28	49
J1550+4001(197,23)	0.31247	1.78	11.4	13.50	14.10	578	577	0.79	106
J1550+4001(97,33)	0.32179	0.82	10.9	12.54	12.91	311	207	1.00	155
J1555+3628(88,11)	0.18930	0.54	10.5	12.38	12.24	254	117	1.12	35
J1617+0638(253,39)	0.15258	2.65	11.5	14.03	14.40	912	747	0.74	104
J1619+3342(113,40)	0.14137	0.19	10.1	12.12	11.76	211	78	1.21	100
J2257+1340(270,40)	0.17675	0.67	10.9	12.78	12.91	348	207	1.00	120
J2345-0059(356,12)	0.25389	0.80	10.9	12.63	12.91	304	207	1.00	48

[a]COS-Halos survey data on 44 galaxies (Tumlinson et al. 2013; Werk et al. 2013). Column 1 lists background QSO and intervening galaxy, following their notation (position angle with respect to QSO and angular separation in arcsec). Columns 2-4 give galaxy redshift, luminosity in L^*, and stellar mass M_* computed from SDSS *ugriz* photometry (Werk et al. 2012) updated by Tumlinson et al. (2013). Column (10) gives the impact parameter R (in kpc) of the QSO sight line relative to galaxy, using angular separation converted to angular-size distance using WMAP-9 ΛCDM cosmological parameters ($h = 0.7$, $\Omega_m = 0.275$, $\Omega_\Lambda = 0.725$) that differ slightly from values in Tumlinson et al. (2013).

[b]Galaxy halo masses M_h (in $M_\odot$) were estimated two ways: Column 5 (old) by abundance-matching (Moster et al. 2010, as used by Tumlinson et al. 2013); Column 6 (new) by modeling luminosity function and halo matching (Tacchella et al. 2013). Virial radii (in kpc) were also estimated two ways: Column 7 (Tumlinson et al. 2013) and Column 8 (this paper eq. [12]) using new halo mass M_h from Column 6 and halo assembly redshift $z_{\rm vir} = z_a$ (column 9).

Table 4. **Statistical Averages[a] for COS-Halos Sample**

Sample	$N_{\rm gal}$	$\langle \log M_* \rangle$ (M_* in $M_\odot$)	$\langle \log M_h^{(\rm old)} \rangle$ (M_h in $M_\odot$)	$\langle \log M_h^{(\rm new)} \rangle$ (M_h in $M_\odot$)	$\langle R_{\rm vir}^{(\rm old)} \rangle$ (kpc)	$\langle R_{\rm vir}^{(\rm new)} \rangle$ (kpc)	$\langle R_{\rm vir}^{(\rm new)}/R_{\rm vir}^{(\rm old)} \rangle$
All Galaxies	44	10.61	12.53	12.55	315	200	0.563
$\log M_* = 10.1 - 10.4$	12	10.23	12.12	11.89	207	81	0.422
$\log M_* = 10.8 - 10.9$	10	10.84	12.62	12.80	309	190	0.613
$\log M_* = 11.2 - 11.5$	7	11.34	13.53	13.97	626	534	0.845

[a]Statistical means of halo masses ($\log M_h$) and virial radii ($R_{\rm vir}$) computed for the two different methods, labeled *old* and *new*, from data in Table 3. Values are shown for all 44 COS-Halos galaxies and for three subsets at low, medium, and high stellar masses (M_*). The last column shows averages of the ratio of $R_{\rm vir}$ in the two methods.

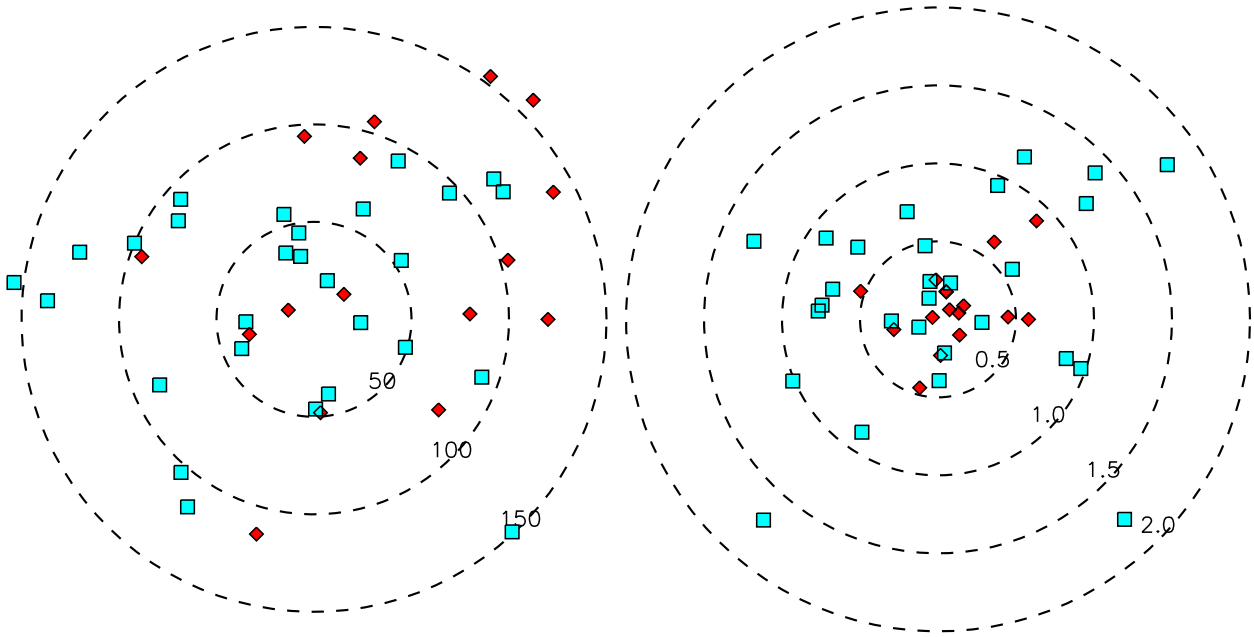

Fig. 1.— Distribution of COS-Halos targets (Tumlinson et al. 2013). *Left Panel*: Impact parameter (R in kpc) and position angle (measured from N to E) of the background AGN relative to 44 galaxies in survey. Blue squares show 28 actively star-forming galaxies, and red diamonds show 16 passive galaxies. These impact parameters have been slightly updated using WMAP-9 cosmological parameters (see text). *Right Panel*: Normalized radial extent, $R/R_{\rm vir}$, relative to the newly computed virial radii (Table 3). Many of the sight lines through star-forming galaxies probe gas outside $R_{\rm vir}$, while *all* of the passive galaxies probe gas at $R < R_{\rm vir}$. This dichotomy suggests the role of feedback from strong galactic outflows in metal transport to the CGM and IGM.